Available online at www.eccomasproceedia.org
Eccomas Proceedia COMPDYN (2017) 441-458

ECCOMAS
Proceedia

COMPDYN 2017
6th ECCOMAS Thematic Conference on
Computational Methods in Structural Dynamics and Earthquake Engineering
M. Papadrakakis, M. Fragiadakis (eds.)
Rhodes Island, Greece, 15–17 June 2017

UNREINFORCED STONE MASONRY UNDER IN-PLANE STATE OF STRESS FROM GRAVITATIONAL AND SEISMIC ACTIONS. MEASURED AND PREDICTED BEHAVIOUR

G.C. Manos[1], **L. Kotoulas**[2]

[1] Professor Emeritus and ex-Director of the Lab. of Strength of Materials and Structures, Aristotle University,

[2] Postgraduate student, Lab. of Strength of Materials and Structures, Aristotle University

Keywords: Stone masonry, In-plane behavior, Gravitational forces, Seismic actions, Limit non-linear behaviour, In-plane behaviour

Abstract. *Unreinforced masonry made of stone and low strength mortar has been used for centuries in forming the structural system of old type buildings as well as monumental structures (such as churches etc.) The behaviour of this type of structural systems that survive today, when subjected to the combined gravitational loads and seismic actions, is still of interest. In this framework, the present work tries to evaluate the limit-state in-plane behavior of stone masonry vertical structural elements. Initially, the behaviour of vertical specimens constructed of stone masonry is presented as observed through a sequence of laboratory tests. These specimens were constructed employing relatively weak mortar that resembles the mortar employed in old-type stone masonry construction. The in-plane loading that was used subjected these specimens to simultaneously vertical and horizontal loads. The possibilities offered by non-linear inelastic numerical analyses as means for examining the performance of such un-reinforced stone masonry vertical structural elements is next examined. Numerical simulation results are presented making use of such non-linear inelastic numerical analyses that are applied to the vertical stone masonry specimens that were tested in the laboratory. Through the comparison of the obtained numerical predictions with the observed behaviour the validity of the numerical approach is discussed.*

Peer-review under responsibility of the organizing committee of COMPDYN 2017.
doi: 10.7712/120117.5431.19535

1. INTRODUCTION

During the last thirty years various parts of Greece have been subjected to a number of damaging earthquakes [15] ranging from Ms=5.2 to Ms=7.2 on the Richter scale. Some of these events, not necessarily the most intense, occurred near urban areas (Manos [7] and [14]). One of the most demanding tasks for counteracting the consequences of all these seismic events was the effort to ensure the structural integrity of old masonry construction, which in many cases they sustained considerable damage as can be seen in figure 1a (Manos et al. [5], [6], [7], [8], [10], [12], [13], [14]). In many cases the observed damage to the stone masonry is amplified by the foundation deformability depicted in figure 1b (Manos et al. [9], [11]). Laboratory testing of masonry structures has utilized in the past complex means such as earthquake simulators [3].

Figure 1a. Stone masonry heavily damaged by the 1995 Kozani earthquake

Figure 1b. Stone masonry heavily damaged by the foundation deformability

In the present study the behaviour of old-type stone masonry construction is initially examined utilizing the triplet test. This is a relatively simple and well known test for contemporary masonry construction using regular masonry units of prismatic shape with planar sides [1]. During this test a small masonry specimen is constructed employing three masonry units and two horizontal mortar joints, as shown in figures 2a and 2b. A vertical load is first applied whereby the two horizontal mortar joints are subjected to an axial normal stress (σ_n) that remains at an almost constant amplitude throughout the duration of the test. Next, the horizontal load is gradually applied (figures 2a and 2b) in a way to produce the desired shear-type loading to the horizontal mortar joints leading eventually to sliding failure between the stones and the mortar joints.

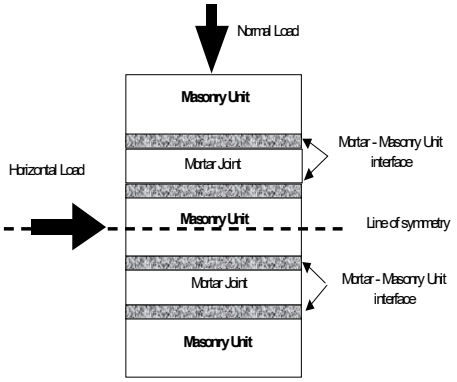

Figure 2a. Test arrangement for a triplet test

Figure 2b. Triplet test performed in the laboratory with natural stones of regular rectangular shape with planar sides

This vertical and horizontal loading applied simultaneously in the way described before creates a stress field for the tested masonry specimen that resembles in this simplified form the stress field in a vertical masonry structural element when apart from the gravitational forces is also subjected to horizontal seismic loads ([2], [16]). Use will be made of this simplified loading arrangement to examine the shear strength of old-type stone masonry construction.

2 SIMPLE TESTS FOR OBTAINING THE SHEAR STENGTH OF STONE MASONRY CONSTRUCTION

A more complex extension of the triplet test described in the introduction was attempted by building four short stone masonry specimens with dimensions in plan approximately 350mm x 250mm and a height approximately 280mm. These specimens were built with stones of approximately 60MPa compressive strength and mortar of average compressive strength approximately equal to 2.0MPa. The used stones were irregular in shape. These specimens were built in such a way so as to form an irregular mortar surface approximately at the mid-height of each specimen. The lower half part of each specimen was rigidly supported to the reaction frame (figure 3, left part blue arrows) whereas the upper half part of each specimen was connected through a metal section to the horizontal electronically controlled servo-actuator in order to be subjected in this way to the horizontal load (figure 3, right part, pink arrows). At the same time, the top side of each specimen was made planar and horizontal in order to host two planar thick steel plates that were separated with a group of sliding cylinders. The vertical load was first applied through a vertical jack placed on top of a load cell that was supported by the top of these two sliding steel plates. The sliding cylinders ensured that the bottom steel plate could slide relatively to the top steel plate with a low friction (coefficient of friction smaller than 4%).

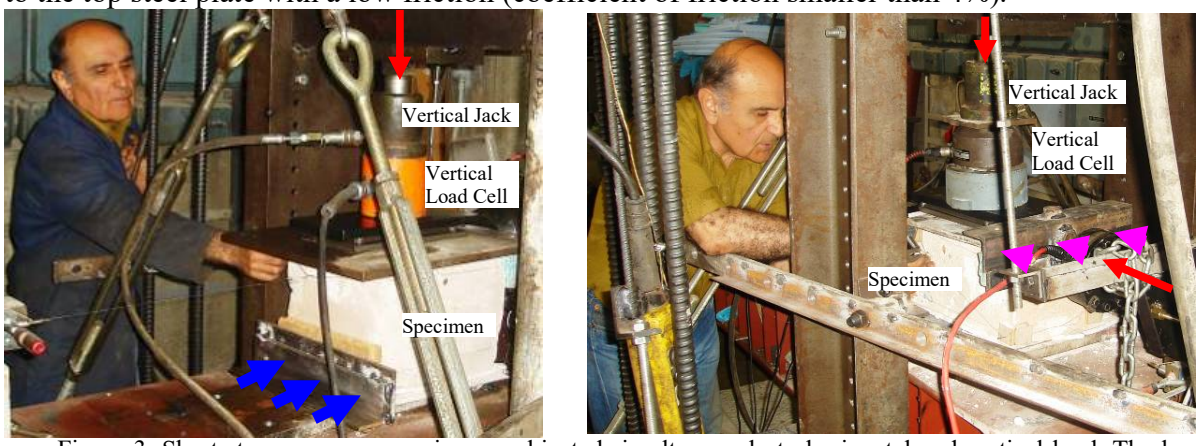

Figure 3. Short stone masonry specimens subjected simultaneously to horizontal and vertical load. The lower half was rigidly supported to the reaction frame (left figure) whereas the top part was loaded horizontally (right figure).

In this way, when the horizontal load was applied after the vertical load the top sliding plate offered very small resistance to the horizontal deformation of the tested specimen, which resisted in this way almost all the horizontal load. Moreover, the way the test specimen was constructed, supported and loaded horizontally the mortar mid-surface was forced to reach a limit-state sliding mode of failure, as will be shown in the following. All specimens were built and all tests were conducted at the laboratory of Strength of Materials and Structures of Aristotle University. The composition of the lime mortar was that of old relatively weak mortars [14].

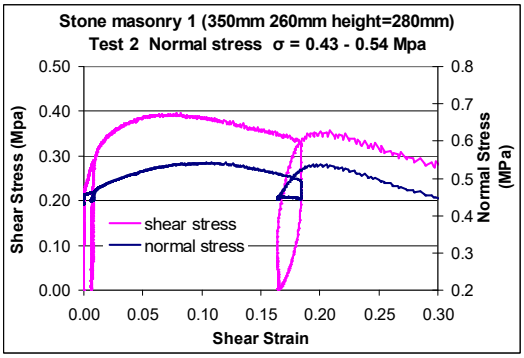

a)

b) Spec. 1

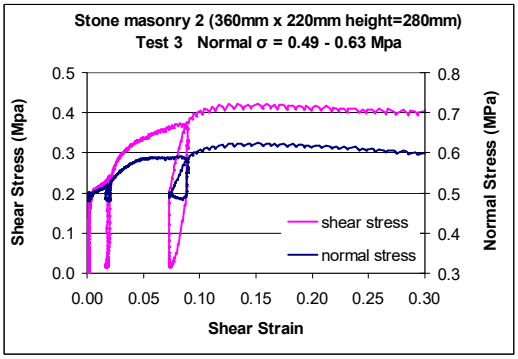

c)

d) Spec. 2

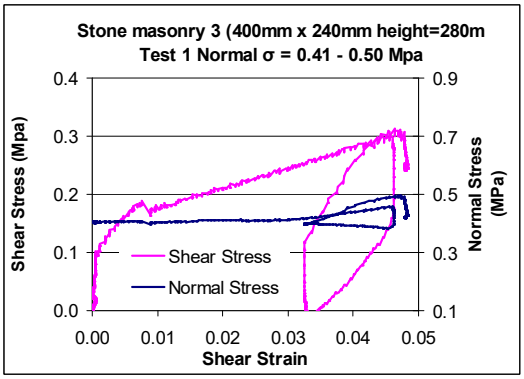

e)

f) Spec. 3

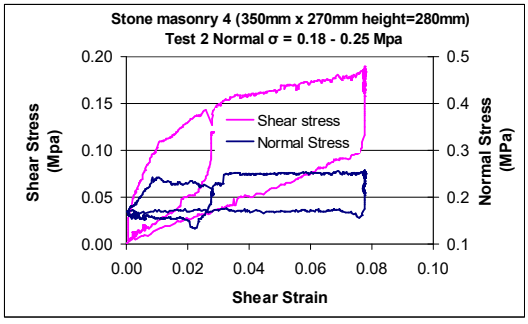

g)

h) Spec. 4

Figure 4. Obtained shear stress limit state and corresponding mode of failure of the four short stone masonry specimens.

The objective of this experimental set-up was designed in an effort to obtain the maximum shear stress at a limit state which represented the sliding failure of the mid mortar surface of

each short stone masonry specimen for a given normal stress regime. For this purpose the variation of the amplitude of the vertical and horizontal load was monitored continuously throughout the test. The average shear and normal stress regime was obtained by dividing the horizontal and vertical load by the horizontal cross-section of each specimen, assuming a uniform normal and shear stress distribution. Moreover, the horizontal displacement of the upper half part of the short stone masonry specimen relative to the lower rigidly supported part was also monitored by a set of displacement transducers throughout the test. An approximation of the corresponding shear strain regime was obtained by dividing this horizontal displacement by the free height of the tested specimen. The obtained normal and shear stress variation for each specimen is plotted in figures 4a, 4c, 4e and 4g against the corresponding shear strain variation. The obtained in each case mode of failure is depicted in figures 4b, 4d, 4f and 4h. As can be seen in all cases the sliding mode of failure was the one that developed in all four specimens. Moreover, in all four tests, depicted in figures 4a, 4c, 4e and 4g, the vertical load was not exactly constant throughout the test, but exhibited a variation which is recorded, with its range (minimum and maximum values) also listed in these figures together with the dimensions of each specimen. From all these measurements a Mohr Coulomb sliding shear failure criterion was derived (Equation 1); it describes the shear strength of the tested stone masonry as a linear function of the applied normal stress.

Mohr Coulomb sliding shear failure criterion $f_v = f_{vo} + 0.45\ \sigma_n$ (1)

Where: σ_n = the compressive stress normal to the sliding surface

f_{vo} = 0.12 Mpa. The shear strength for zero normal stress.

The shear strength values predicted according to the above Mohr Coulomb failure criterion are listed in Table 1 for each one of the tested specimens. In the same table the observed shear strength is also listed as well as the ratio between measured and predicted shear strength values. As can be seen these ratio values are close to unity a fact that demonstrates the validity of the Mohr Coulomb failure criterion derived in the way described above.

Table 1. Summary of test results and the corresponding Mohr Coulomb failure criterion.

	Normal Stress σ_n (Mpa)	Predicted $f_v = f_{vo} + 0.45\ \sigma$ (Mpa)	Measured value f_v (Mpa)	Ratio Measured f_v / Predicted f_v
Specimen 1	0.53	0.359	0.396	1.103
Specimen 2	0.61	0.395	0.41	1.038
Specimen 3	0.46	0.327	0.305	0.933
Specimen 4a	0.30	0.255	0.20	0.784
Specimen 4b	0.54	0.363	0.375	1.033

Following these initial samples, another sequence of tests was performed aimed at quantifying the Mohr-Coulomb failure envelope representing old stone masonry that was used to construct five (5) vertical stone masonry wall specimens, as shown in figure 5a. These wall specimens are of the same dimensions (*length equal to* $\boldsymbol{\ell}$ *=1500 mm height* $\boldsymbol{h}$*=1400 mm and thickness* $\boldsymbol{t}$*= 500 mm*) and were built at the Laboratory of Strength of Materials and Structures of Aristotle University employing the same stone masons (figure 5a). All these wall specimens were built with the same natural stones provided by a quarry near Tsotili at the prefecture of Kozani. The compressive cubic strength of these stones was found to be equal to approximately

60MPa. Four different mortars (M1, M2, M3 and M4) were used for building each one of these all of them resembling mortars used in traditional stone masonry. The compressive strength of these four mortars is listed in table 2, as was found from cubic specimens tested eight (8) months after casting. As can be seen in this table M1 is a relatively weak mortar whereas M2 and M4 are relatively strong. Together with these vertical wall specimens a number of new short pier specimens were also built with dimensions in plan 500mm x 500mm and a height of 300mm (figure 5b). These new short piers were built by the same masons that built the larger vertical walls of figure 5a employing the same materials and the same construction technique. Each one of these short piers is characterized with the name of the mortar that was used (M1, M2, M3 and M4).

Table 2. Summary of compressive strength of the mortars used in the stone masonry construction.

Eight (8) months old	M1	M2	M3	M4
Cubic compressive strength	0.34(Mpa)	3.04(Mpa)	1.44(Mpa)	2.87(Mpa)

Figure 5a. Vertical stone masonry wall specimens with a length equal to **l**=1500 mm height **h**=1400 mm and thickness **t**= 500 mm.

Figure 5b. Short piers with dimensions in plan 500mm x 500mm

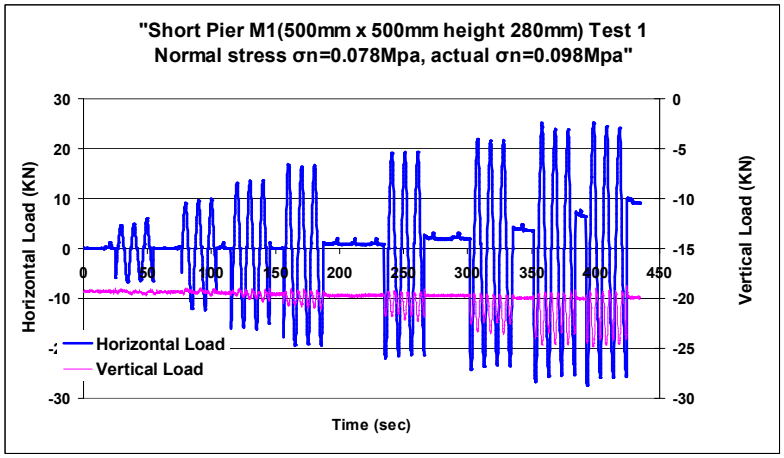

Figure 6. Cyclic horizontal load sequence with the simultaneous application of vertical load for the new short pier specimens.

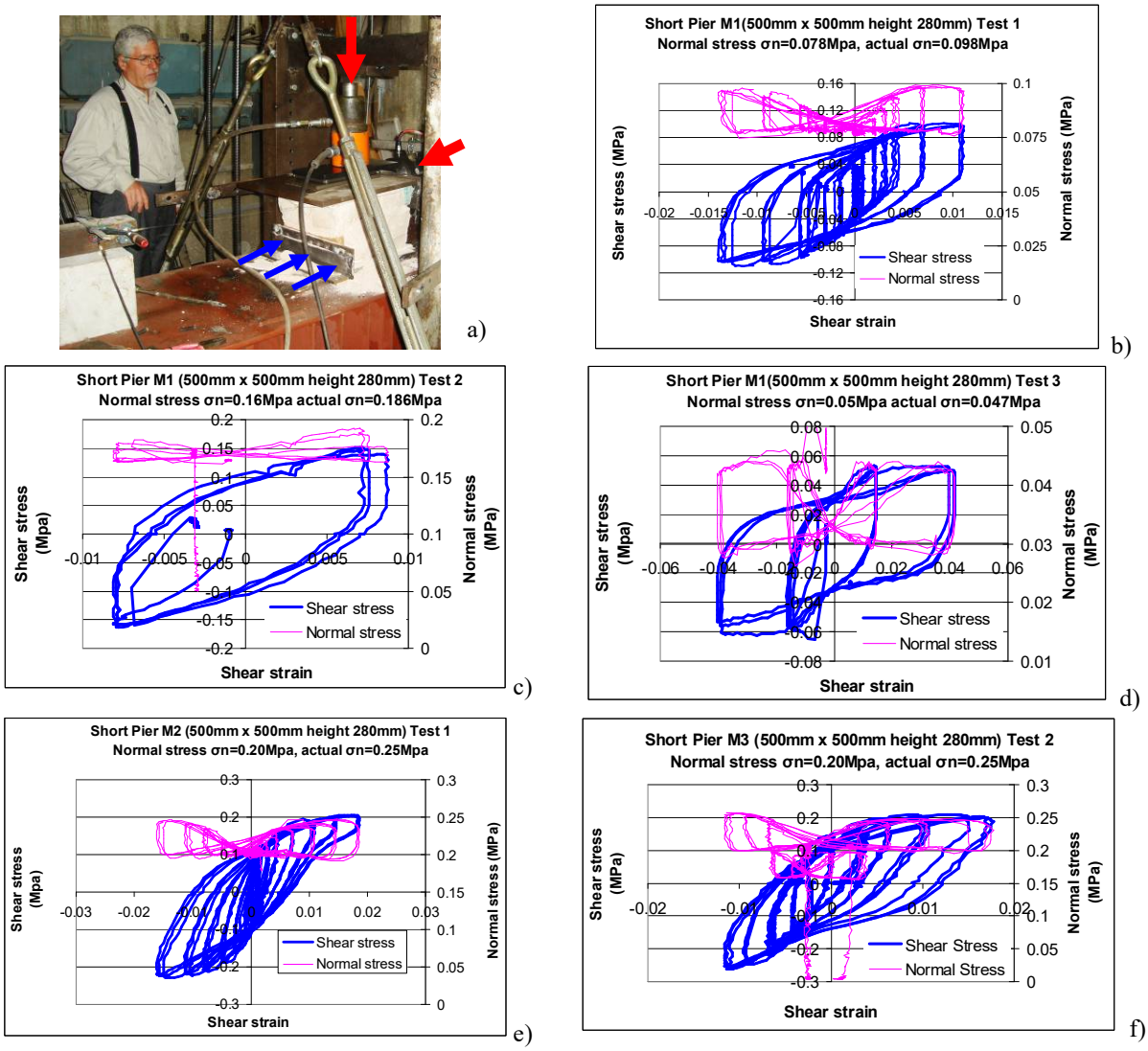

Figure 7. Short stone masonry specimens subjected simultaneously to horizontal and vertical load. Shear stress versus shear strain cyclic response for the short pier specimens M1, M2 and M3.

These new short piers were tested in the same way as described before (figure 7a and figure 3). They were built in a way capable of forming a sliding mortar surface at approximately the mid-height of each specimen (figure 5b). The upper half of each of these short pier specimens was connected to the hydraulic servo-actuator in such a way as to be subjected to cyclic horizontal load simultaneously with approximately constant vertical compressive load. Similarly, the lower half of each specimen was connected to the rigid frame in a way as to be able to sustain this simultaneous loading sequence. The frequency of the cyclic horizontal loading was kept constant equal to 0.1Hz throughout this loading sequence of the short piers. The level of vertical load was varied from test to test. Figures 8a to 8e depict the observed response in terms of average shear stress against the corresponding shear strain. In each one of these figures the variation of the average normal stress is also indicated.

Figures 7b, 7c and 7d depict the observed shear stress versus shear strain cyclic response for the short pier specimen M1 for various levels of compressive normal stress whereas figures 7e

and 7f depict the observed shear stress versus shear strain cyclic response for the short pier specimens M2 and M3, respectively. Based on the obtained cyclic horizontal load response results of the new short pier specimens the Mohr Coulomb sliding shear failure criterion takes the following form:

$$f_v = f_{vo} + \mu\, \sigma_n \quad (2)$$

Where: μ = the dynamic friction coefficient = 0.5932

σ_n = the compressive stress normal to the sliding surface

f_{vo} = The shear strength for zero normal stress

f_{vo} = 0.0474MPa for specimen M

f_{vo} = 0.070MPa for specimens M2 and M3.

3 NUMERICAL SIMULATIONS

Two different modeling strategies are applied here for the numerical simulation of the stone masonry, namely, a macro-modeling and a micro-modeling strategy. In macro-modeling strategy the stone masonry is simulated as plane stress elements with homogenised, single material properties (figure 8a). In micro-modeling strategy the constituents of the masonry infill are simulated separately (mortar joints, and masonry units, figure 8b), and different mechanical properties are assigned in each of these numerical representations as will be explained in the following.

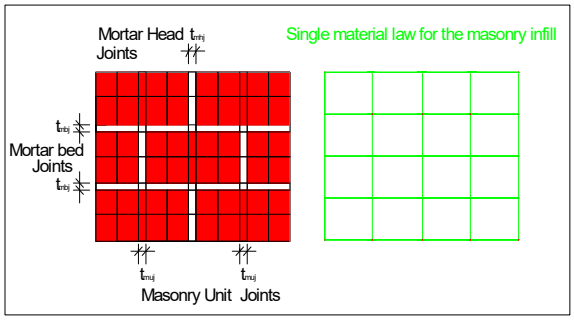

Figure 8a. Masonry infill simulation with macro-modeling strategy

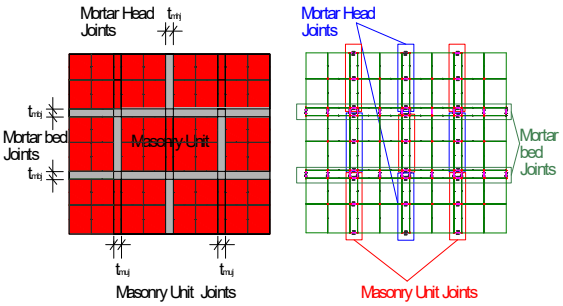

Figure 8b. Masonry infill simulation with micro-modeling strategy

3.1.Numerical simulation of the triplet test for short stone masonry piers.

3.1.1. Macro-modeling approach.

In figures 9 to 16 the numerical simulation of the behaviour of the short pier and its loading conditions, described in section 2, is depicted utilizing the ABAQUS commercial software package [4]. Figures 9 and 10 show the used finite element mesh and the loading and support conditions that resemble the actual loading and support conditions of the short pier test sequence as described in section 2. The deformable part of the mesh in figure 9 is the one designated with blue

colour whereas the non-deformable part is designated with white colour. The numerical prediction of the bearing capacity of this pier in terms of shear stress is shown in figure 11 and it compares quite well (figure 16) with the measured maximum shear capacity (figure 12) that was observed during the cyclic test for this short pier (see also figure 7). Figure 13 shows the predicted by the non-linear inelastic analyses plastic strains of the deformable part; the observed damage pattern for the short pier is shown in figure 14. As can be seen good agreement can be observed. Finally, figure 15 depicts the distribution of the principal tensile stresses that compares well both with the plastic strain distribution and the observed damage.

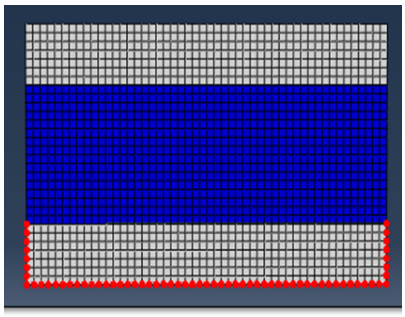

Figure 9. Fixing the low part of the short pier numerical simulation in the same way that the actual test specimen was supported.

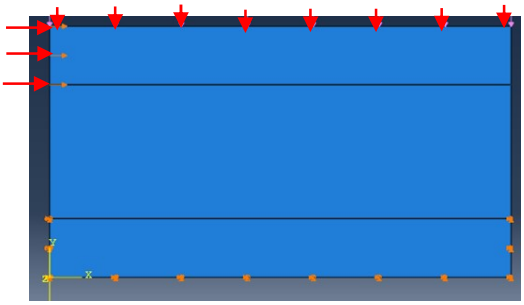

Figure 10. Fixing of the low part of the numerical simulation of the short pier in the same way that the actual test specimen was supported together with the application of uniform compression at the upper boundary equal to 0.16MPa.

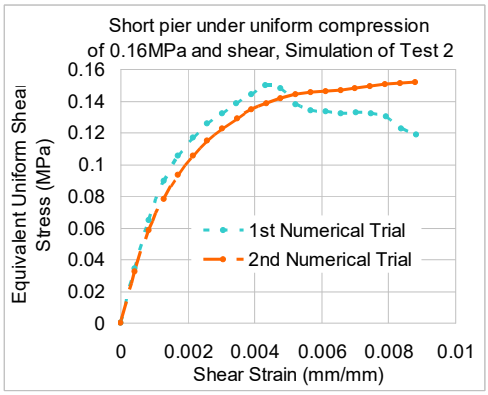

Figure 11. Numerical prediction of the monotonic response of the short pier in terms of shear stress (τ) /shear strain (γ) with simultaneous normal compressive stress 0.16MPa

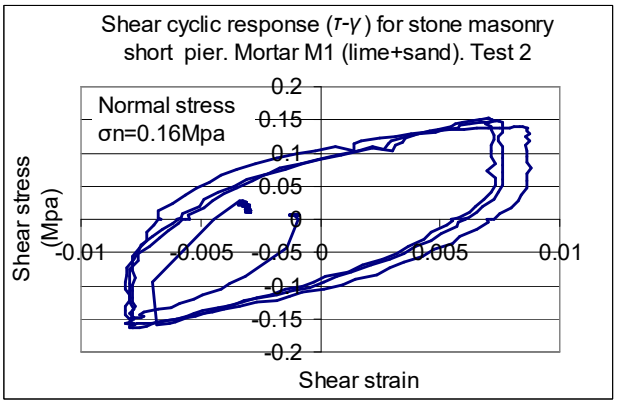

Figure 12. Measured cyclic response of the short pier in terms of shear stress and shear strain when it is simultaneously compressed with a normal stress equal to 0.16MPa

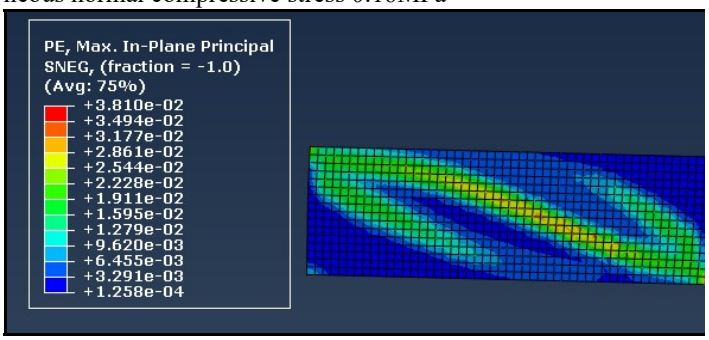

Figure 13. Distribution of predicted plastic strains

Figure 14. Observed damage pattern

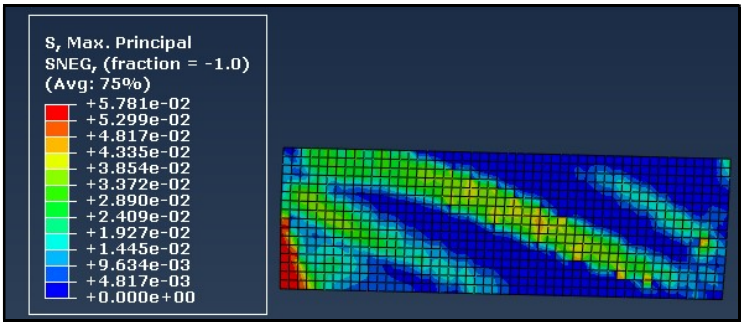

Figure 15. Distribution of tensile principal stresses at maximum load

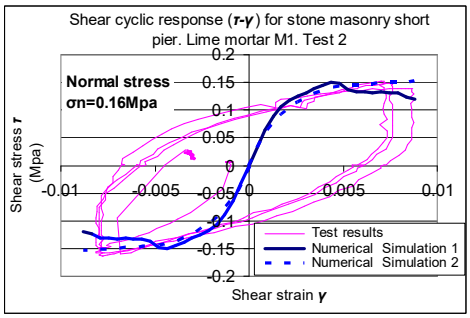

Figure 16. Measured and predicted cyclic response of the short pier

3.1.2. Micro-modeling approach.

Initially, a parametric study was conducted simulating numerically the triplet set ,described in section 1 (figure 2a), which consists of three stone masonry units and two horizontal mortar joints, as shown in figure 17. In one numerical model the mortar joint was simulated with one layer of finite element in its thickness (figure 17a) whereas in an alternative numerical model (17b) two layers of finite elements were employed in the thickness of the horizontal mortar joint. Moreover, a friction layer was introduced in every contact surface between the mortar joint and the stone as indicated in figure 17c. In the numerical models depicted in figures 17a and 17b there are four such friction layers. The mechanical properties of the stone are dictated by its Young's modulus and Poisson's ratio (E= 30GPa, ν=0.13) and is assumed to remain elastic. The non-linear plastic behaviour is assumed to occur in the mortar joints, which is believed to be a realistic assumption for practical purposes. This non-linear numerical simulation can capture both the friction-sliding response between the mortar joint and the stone as well as the plastification of the mortar joint itself.

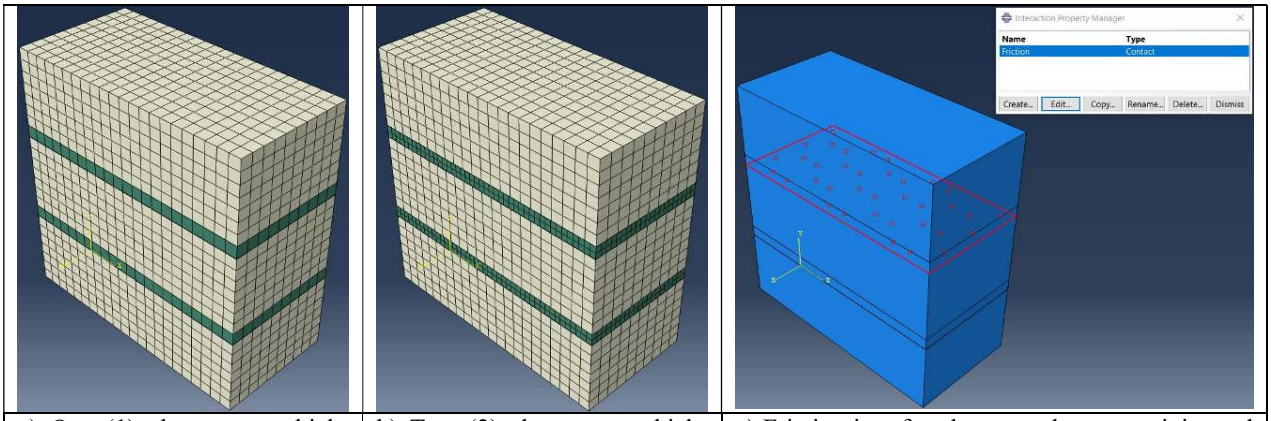

a) One (1) element per thickness of the mortar joint	b) Two (2) element per thickness of the mortar joint	c) Friction interface between the mortar joint and the mesh representing the stone

Figure 17. Micro-modeling of the triplet test.

A number of parametric numerical studies were performed to ensure the realism of this numerical simulation. The parameters that were employed were a) the friction characteristics of the friction layers, b) the mortar characteristics in terms of compression and tensile behaviour of the mortar joint and c) the dilatancy of the mortar joint through the dilation angle. In all these numerical tests the normal pressure was kept constant equal to 3.0MPa.

Initially, a variation of the friction coefficient was studied (μ from 0.75 to 2.0), keeping the dilation angle constant (dilation angle = 5) and assigning constant mortar strength characteristics (tensile strength = 0.9MPa).

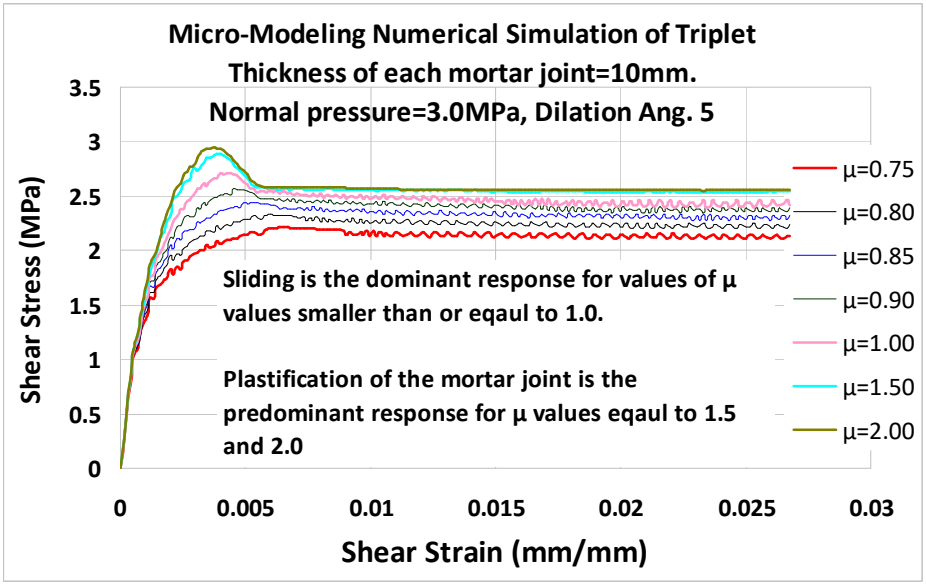

Figure 18. Triplet shear stress – shear strain monotonic load response. Variation of the friction coefficient.

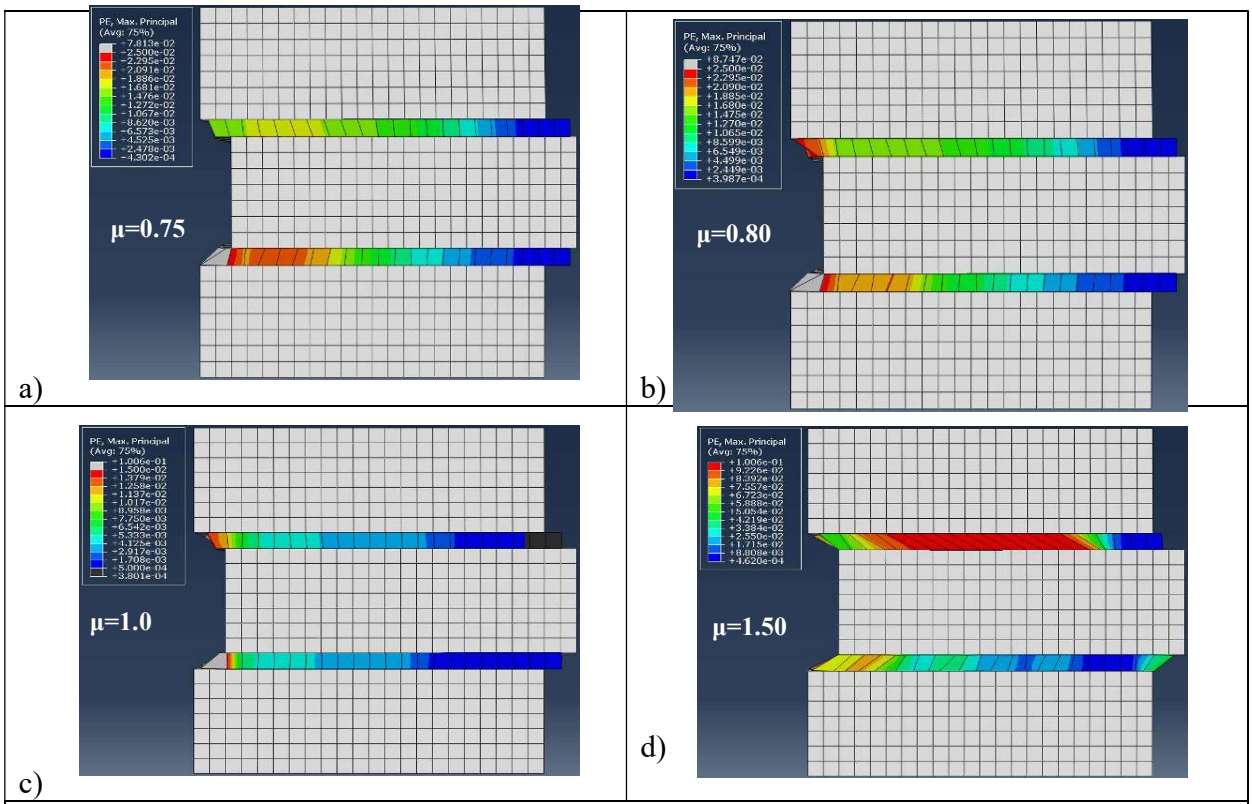

Figure 19. Plastic strain of the mortar joints for various values of friction coefficient for the friction layers

Figure 18 depicts the shear stress – shear strain response as resulted from a horizontal loading that increases in a monotonic way. Figure 19 depicts the plastic strains that develop at the mortar joints at the end of the monotonic load sequence (shear strain=0.27%) for various values of friction coefficient for the friction layers (μ=0.75, μ=0.80, μ=1.0, μ=1.5). As can be seen in figure 18, the increase in the value of the friction coefficient (μ) from 0.75 to 1.5 resulted, as expected, in an increase in the corresponding shear strength value. However, this increase also resulted in a gradual increase of the plastification of the mortar joint. This can also be seen in figure 19. In figure 19a (μ = 0.75), the sliding of the mortar joint to stone interface is most predominant response with the plastification of the mortar joint itself being less significant than the sliding response. On the contrary, in figure 19d (μ = 1.50) the plastification of the mortar joint becomes more significant than the sliding response. This is also demonstrated by comparing the shear stress – shear strain response curve for 19d for μ = 1.50 in figure 18 with the corresponding response for μ = 2.00. This is due to the fact that the increase in the friction coefficient resulted in prohibiting the sliding and thus the response is dominated by the plastification of the mortar joint, which has already reached its limit strength. This is the reason that only very small increase in the shear strength can be seen when the value of the friction coefficient becomes equal to 2.0 instead of 1.5 in figure 18.

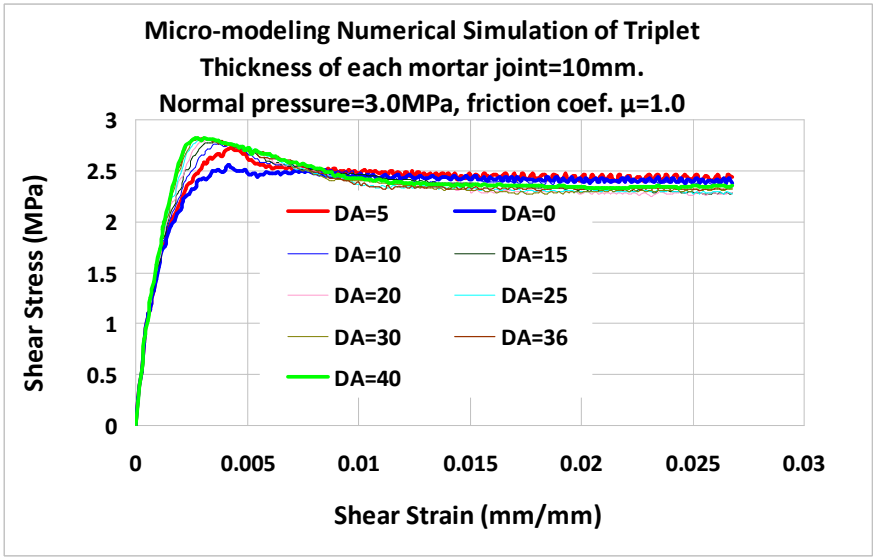

Figure 20. Triplet shear stress – shear strain monotonic load response. Variation of the dilation angle.

Next, a variation of the dilation angle was studied (dilation angle from 0.1 to 40), keeping the friction coefficient constant (μ = 1.0) and assigning again constant mortar strength characteristics (tensile strength = 0.9MPa). The obtained triplet shear stress – shear strain monotonic load response is shown in figure 20. As can be seen, the increase in the value of the dilation angle results in an increase in the value of the shear strength. Moreover, the increase in the value of the dilation angle also results in a more "smooth" response.

In order to examine the micro-modeling approach even further, the numerical study was extended to include the cyclic nature of the horizontal loading. As described in section 2, this was investigated during testing of the new short pier specimens (see figures 6 and 7). The triplet numerical model with one finite element to represent the mortar joint and with a friction coefficient value μ=2.0 subjected to 3.0MPa normal stress was employed in all cases of this study keeping the tensile strength of the mortar the same (0.9MPa). In figure 21 the cyclic response is com-

pared to the monotonic response when the analysis was performed in single precision in both cases. Next, the following alterations were also studied. First to the previous numerical model with one finite element representing the mortar joint a double precision numerical analysis was performed. This did not result in any noticeable variation in the predicted triplet shear stress – shear strain cyclic load response. Secondly, apart from the double precision of the analysis the mortar joint was numerically modeled with two elements in its thickness. The model with two elements in the mortar joint thickness could not be solved in single precision. As can be seen in figure 21, the introduction of two elements for the mortar together with the double precision in the solution algorithm resulted in a noticeable variation of the predicted triplet shear stress – shear strain cyclic response.

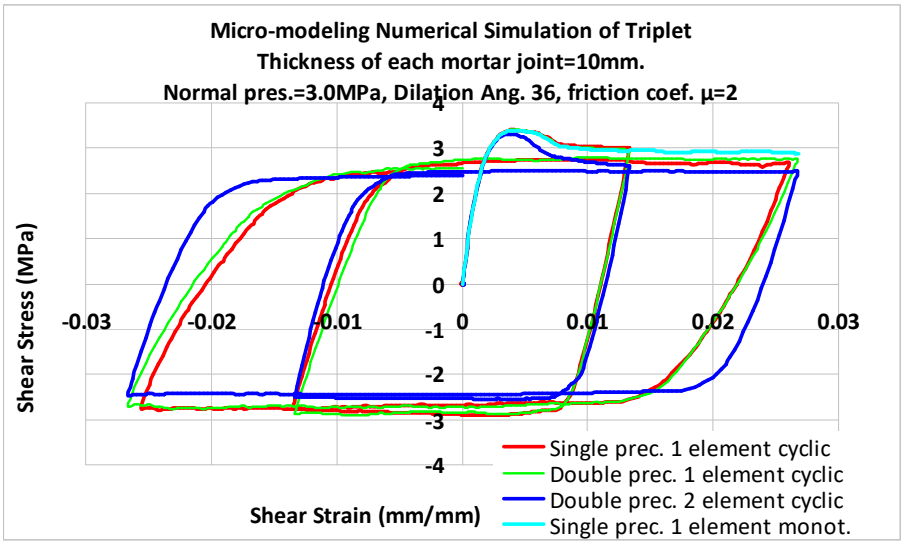

Figure 21. Triplet shear stress – shear strain cyclic load response. Variation of precision of the solution.

3.2. Macro-modeling numerical simulation of a vertical stone masonry pier.

A stone masonry almost "square" pier is examined next having a length equal to ℓ=1500 mm, a height equal to h=1400 mm and a thickness equal to t= 500 mm, thus a length over height ratio (ℓ/h) equal to 1.071 (quite close to 1.0). This square pier specimen was built at the laboratory of Strength of Materials and Structures of Aristotle University with the same stones and mortar that were used to construct the new short pier specimen presented before (figure 5a, section 2). This square pier specimen was subjected to a uniform compression equal to approximately 0.12Mpa at its upper boundary, by applying twin vertical forces on a rigid steel beam resting at the top of this specimen as is shown in figures 22a and 22b. The horizontal load was next applied, as is also shown in figures 22a and 22b. This horizontal load results from the imposed horizontal displacement at the upper boundary which reaches a value equal to 10mm at the final stages.

Figure 22a depicts the experimental set up showing the resulting horizontal load at the top of the stone masonry pier whereas figure 22b is the corresponding numerical simulation. More information on the loading arrangement is provided by Manos (2016). Figures 15a and 15b depict the variation of the shear stress versus the shear strain (blue line). The horizontal load was applied in a cyclic low-frequency seismic-type manner.

In figures 23a and 23b the variation of the compressive axial stress normal to the bed-joint is also plotted (pink line using the far right axis with the negative values). As can be seen in figure 23a, the maximum shear stress was equal to 0.09MPa for Test 6. For this test the corresponding average axial stress value was equal to -0.16MPa (the minus sign indicates compression) exhibiting a relatively small variation around this value during cyclic loading. On the contrary, the variation of the axial stress during cyclic test 7 reached a value equal to -0.26MPa that corresponded to a shear stress value equal to 0.15MPa. At the reverse cycle, the axial stress value was equal to -0.12MPa when the corresponding shear stress value was equal to 0.09MPa, as was the case for test 6.

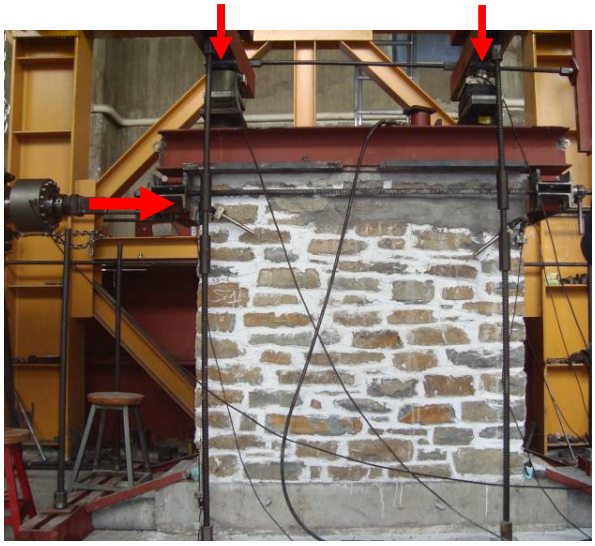

Figure 22a. Stone masonry wall specimen S1M1. Loading arrangement being utilized.

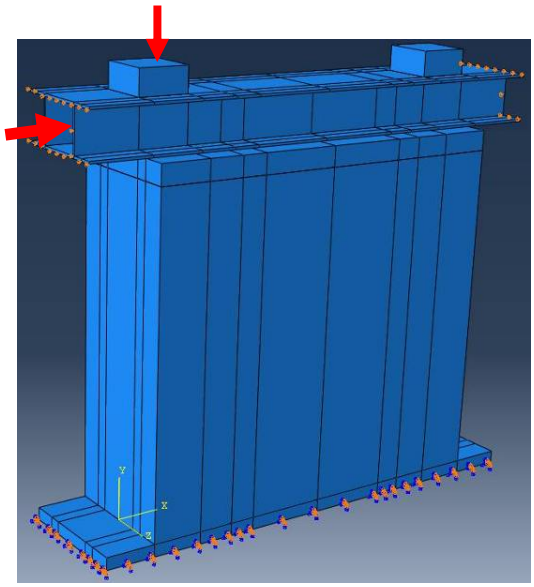

Figure 22b. Numerical simulation of the loading arrangement for wall specimen S1M1.

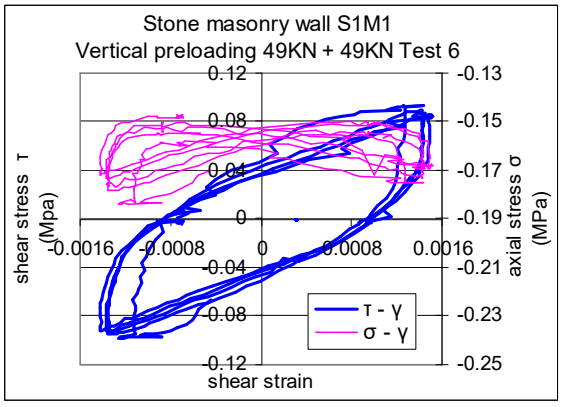

Figure 23a. Variation of the measured shear / axial stress versus the shear strain. Test 6.

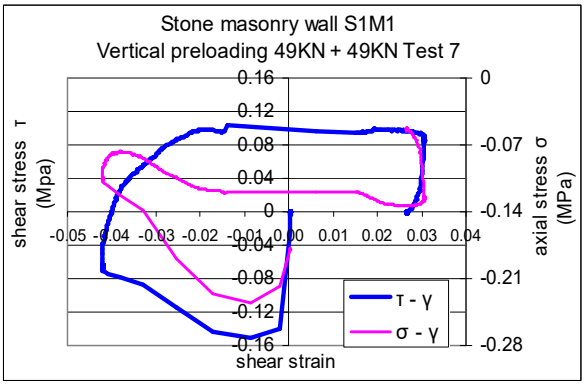

Figure 23a. Variation of the measured shear / axial stress versus the shear strain. Test 7.

The measured variation of horizontal load (H) versus horizontal displacement (δ) at the top of the specimen for tests 6 and 7 is depicted in figure 16. In the same figure the numerical predictions are also plotted as resulting from the non-linear numerical simulation. As can be seen, the comparison between predicted and observed H-δ response is reasonably good for Test 6. For test 7

there is a distinct difference between observed and predicted response when the horizontal load attains negative values. This is attributed to the variation of the vertical load at this stage of the experiment that reached much higher absolute values, as already mentioned before on the basis of figure 22b. This was not accounted for up to now in the numerical simulation that kept constant throughout the vertical load at each location. Additional numerical simulations are required to account for the observed vertical load variation. The numerically predicted horizontal deformation pattern resulting from the non-linear simulation is depicted in figure 24; this deformation pattern is for the maximum horizontal load equal to 57.71KN, which was reached for horizontal displacement at the top of the pier equal to δ=1.85mm.

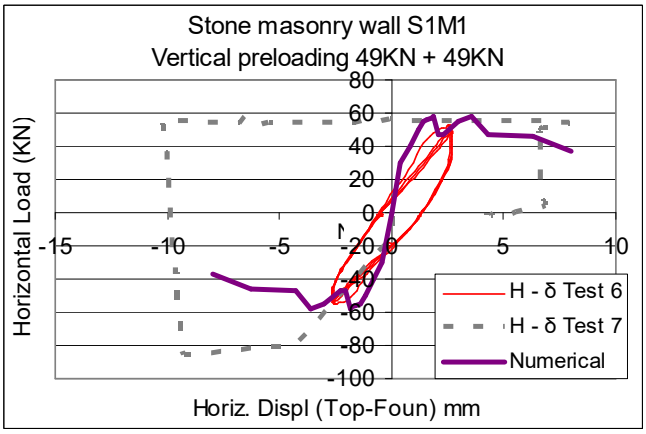

Figure 24. Variation of the horizontal load versus the horizontal displacement at the top. Tests 6, 7 together with numerical predictions.

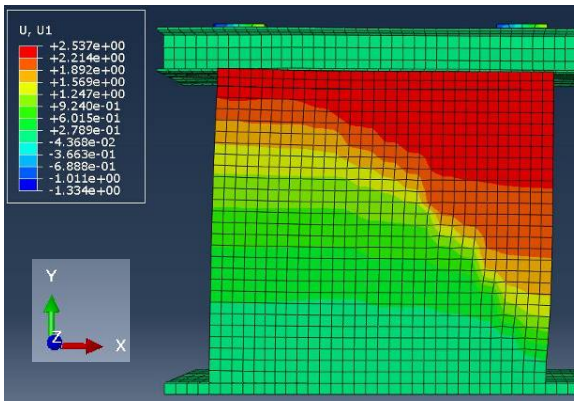

Figure 25. Numerically predicted horizontal deformations for the stone masonry specimen. Maximum value at top 1.85mm.

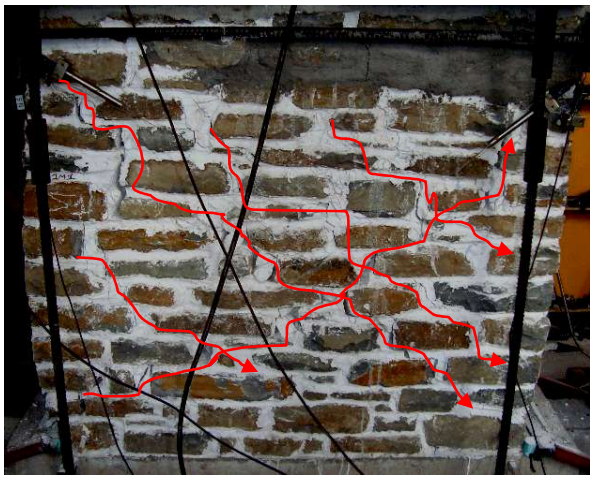

Figure 25. Diagonal cracks that developed in the stone masonry specimen S1M1.

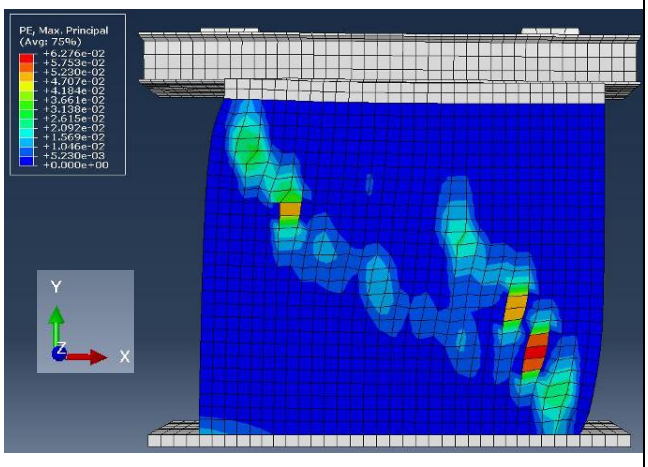

Figure 26. Distribution of numerically predicted plastic strains for H = 43,41 KN Ux = 6,58 mm

Figure 25 depicts the damage patterns in the form of wide diagonal cracks that were formed in this stone masonry wall specimen (S1M1) and were photographed after the end of Test 7. Figure 26 depicts the distribution of the plastic strains that developed in the non-linear numerical simulation when the horizontal load dropped for the first time from its maximum value to 49.96KN and horizontal displacement at the top of the pier reached a value equal to δ=2.4mm. As can be

seen, the formation of the observed diagonal crack pattern is to a certain extend predicted by the non-linear numerical simulation.

4 CONCLUSIONS

- The importance of employing realistic limit-state criteria to be utilized in assessing the bearing capacities of unreinforced stone masonry structural elements is studied together with a summary presentation of relatively simple laboratory testing that can be employed for this purpose.
- The possibilities offered by non-linear inelastic numerical analyses as alternative means for examining the performance of unreinforced stone masonry structural elements is briefly presented. In addition, numerical simulation results are also presented, which were obtained from such non-linear inelastic numerical analyses. The objective here is to numerically simulate the performance of masonry specimens that were subjected to relatively simple laboratory testing. Successful predictions of the observed performance are means to increase the confidence in these numerical tools before employing them in more complex structural formations.
- For this purpose use is made of experimental set-ups employing relatively simple stone masonry specimens of prototype dimensions which were constructed with materials resembling old stone masonry. These specimens were subjected to in-plane combined compression, shear and flexure in such a way as to develop stress fields that are similar to the state of stress prototype stone masonry structural elements develop during combined gravitational forces and seismic actions. The obtained measured behaviour from these tests is then utilized to validate the employed non-linear numerical simulations.
- As was demonstrated from these comparisons a realistic estimate was obtained of the observed seismic type behaviour by these non-linear numerical simulations. Following further validation these non-linear simulations will next be employed in more complex structural components.

ACKNOWLEDGEMENTS

The authors would like to thank Dr, V. Kourtidis and Th. Koukouftopoulos for their assistance during the laboratory testing. Moreover, they wish to acknowledge the assistance of Civil Engineer N. Parcharidis during the numerical simulations.

- To the memory of Ray W. Clough, Professor Emeritus of the University of California, at Berkeley, U.S.A.

REFERENCES

[1] Bernardini A, Modena C, Turnsek V, Vescovi U (1980) A comparison of three laboratory test methods used to determine the shear resistance of masonry walls" Proc. 7th WCEE, vol 7, IAEE, Istanbul, pp 181–184.

[2] European Committee for Standardization, Euro-code 6 (2005); "Design of Masonry Structures, Part 1-1:General Rules for Building. Rules for Reinforced and Un-reinforced Masonry", EN 1996-1-1:2005.

[3] Gulkan P., Clough R.W., Manos G.C. and Mayes R.L., (1990), "Seismic Testing of Single-story Masonry Houses : Parts 1&2", Journal of Str. Eng. ASCE, Vol. 116, No 1, January 1990, pp. 235-274.

[4] Hibbitt, Karlsson, Sorensen. Inc. ABAQUS user's manual volumes I–V and ABAQUS CAE manual. Version 6.10.1. Pawtucket, USA; 2010.

[5] Manos G.C., Soulis V., Diagouma A. (2008) "Numerical Investigation of the behaviour of the church of Agia Triada, Drakotrypa, Greece", Journal in Advances in Engineering Software 39, 284-300.

[6] Manos G., Soulis V., Felekidou O., Matsou V. (2010) "A Numerical Investigation of the Dynamic and Earthquake Behaviour of Byzantine and Post-Byzantine Basilicas", 9th U.S. and 10th Canadian Earthq. Eng. Conf., Canada.

[7] Manos G. C., (2011) "Consequences on the urban environment in Greece related to the recent intense earthquake activity", Int. Journal of Civil Engineering and Architecture, Volume 5, No. 12 (Serial No. 49), pp. 1065–1090.

[8] Manos G.C., Soulis V., Karamitsios N. (2012) "The Performance of Post-Byzantine churches during the Kozani-1995 Earthquake – Numerical Investigation of their Dynamic and Earthquake Behavior", 15WCEE, Portugal.

[9] Manos, G.C, Kotoulas, L., Matsou, V., Felekidou, O. (2013a), "Dynamic behaviour of Greek Post-Byzantine churches with foundation deformability and evaluation of their earthquake performance", CompDyn2013, 12-14 June 2013, Greece.

[10] Manos G. C. & Karamitsios N. (2013b), "Numerical simulation of the dynamic and earthquake behavior of Greek post-Byzantine churches with and without base isolation", Earthquake Engineering Retrofitting of Heritage Structures, Design and evaluation of strengthening techniques, pp. 171-186, Edited By: S. Syngellakis, Wessex Institute of Technology, UK, ISBN: 978-1-84564-754-4, eISBN: 978-1-84564-755-1, 2013.

[11] Manos G.C. and Kotoulas L. (2014), "Earthquake Performance of Greek Post-Byzantine Churches with Foundation Deformability " Proc. 2nd Int. Conf. on Protection of Historical Constructions, pp. 297-303, 2014, ISBN 978-975-518-361-9.

[12] Manos G. C., Kotoulas L., Felekidou O, Vaccaro S. and Kozikopoulos E., (2015a) "Earthquake damage to Christian Basilica Churches – Application of an expert system for the preliminary in-plane design of stone masonry piers", Int. Conf. STREMAH 2015.

[13] Manos G.C. & Kozikopoulos E. , (2015b) "The dynamic and earthquake response of Basilica Churches in Kefalonia-Greece including soil-foundation deformability and wall detachment", CompDyn2015, Krete-Greece, 2015.

[14] Manos G.C., (2016), "The Seismic Behaviour of Stone Masonry Greek Orthodox Churches" Journal of Architecture and Engineering, Vol. 1, Issue 1, March 2016, pp. 44-53, http://aej.spbgasu.ru/index.php/AE/index.

[15] Provisions of Greek Seismic Code with revisions of seismic zonation", Government Gazette, Δ17α /115/9/ΦΝ275, No. 1154, Athens, 12 Aug. 2003.

[16] Tomaževič M., 2009 "Shear resistance of masonry walls and Eurocode 6: shear versus tensile strength of masonry", Materials and Structures, August 2009, Volume 42, Issue 7, pp 889-907